JOURNAL OF GEOPHYSICAL RESEARCH, VOL. 112, A09201, doi:10.1029/2007JA012435, 2007

Electron pitch angle distributions as indicators of magnetic field topology near Mars

D. A. Brain,[1] R. J. Lillis,[1] D. L. Mitchell,[1] J. S. Halekas,[1] and R. P. Lin[1]

Received 30 March 2007; revised 4 May 2007; accepted 29 May 2007; published 6 September 2007.

[1] We have analyzed electron angular distributions recorded near Mars over a period of 7 years in order to constrain the topology of magnetic field lines near Mars. We used 63 million pitch angle distributions of 115 eV electrons measured at ~400 km altitudes by the Mars Global Surveyor (MGS) spacecraft and classified them according to their shape. Closed magnetic field lines are associated with the Martian crustal magnetic fields and are identified on the nightside by the presence of plasma voids or two-sided loss cones (trapped distributions). Trapped distributions on the nightside are most often observed in regions surrounding moderate or strong crustal fields, indicating a source process such as reconnection populates the outer layers of closed magnetic field regions. Open magnetic field lines are identified in regions of strong crustal magnetic field by the absence of field-aligned electrons returning from the planet (loss cones). In regions far from crustal sources many field lines intersect the collisional atmosphere. On the Martian dayside, closed field lines are identified by the presence of trapped or fully isotropic distributions, and they occur at times when ionospheric photoelectron features are evident in MGS electron energy spectra. Variability of the dominant pitch angle distribution shape in certain regions suggests that Martian magnetic field topology is dynamic and is controlled by external conditions.

Citation: Brain, D. A., R. J. Lillis, D. L. Mitchell, J. S. Halekas, and R. P. Lin (2007), Electron pitch angle distributions as indicators of magnetic field topology near Mars, *J. Geophys. Res.*, *112*, A09201, doi:10.1029/2007JA012435.

1. Introduction

[2] Collisonless plasmas are constrained to flow along and with field lines in situations where the frozen-in condition is satisfied (i.e., the plasma has high electrical conductivity). Therefore the topology of a field line determines the regions to which a given plasma population has access, assuming that plasma motion occurs on timescales that are short relative to the timescale for the system to change and that the drift motion of particles across field lines is small. In any system with two sources of magnetic field, three different field topologies are possible. At Earth where the global dynamo magnetic field interacts with the passing interplanetary magnetic field (IMF), *Vasyliunas* [1975] has described the three types of field line as closed (connected at both ends to Earth); open (connected at one end to Earth and at one end to the IMF); and unconnected (connected at both ends to the IMF). Changes in magnetic field topology via magnetic reconnection or merging allow magnetically isolated plasma populations to mix, and result in the conversion of magnetic energy to kinetic energy of plasma particles. Reconnection is thought to be responsible for a variety of solar system phenomena, including solar flare events and substorms in Earth's magnetosphere [*Priest and Forbes*, 2000].

[3] Like at Earth, magnetic fields near Mars have three possible field topologies resulting from the interaction of strong crustal magnetic fields with the solar wind (Mars lacks a significant global dynamo field). Crustal fields measuring more than 50 nT at 400 km altitudes are concentrated in one region of the southern hemisphere [*Acuña et al.*, 2001], and are detectable to altitudes of 1300 km or more [*Mitchell et al.*, 2001a; *Brain et al.*, 2003]. Weaker fields are present in other parts of the Southern Highlands [*Acuña et al.*, 1998, 1999; *Connerney et al.*, 2001], and very weak (<10 nT) fields have been detected in some locations in the northern hemisphere [*Lillis et al.*, 2004; *Connerney et al.*, 2005; *Mitchell et al.*, 2007]. In regions lacking significant crustal magnetic fields the Martian solar wind interaction resembles that at Venus [*Cloutier et al.*, 1999] or comets. The IMF carried by the solar wind drapes around the conducting ionosphere on the dayside of the planet, and is stretched into a two-lobed induced magnetotail on the nightside. Unlike Venus or comets, however, the topology of magnetic fields near Mars should be quite complex, with closed loops of crustal magnetic field, open field lines connecting the crust to the IMF, and draped field lines (Figure 1). The presence of open field lines enables access of solar wind particles to the atmosphere in regions otherwise isolated by crustal fields, and provides avenues by which ionospheric plasma can escape into the solar wind. Topology is therefore relevant

[1]Space Sciences Laboratory, University of California, Berkeley, California, USA.

0148-0227/07/2007JA012435$09.00

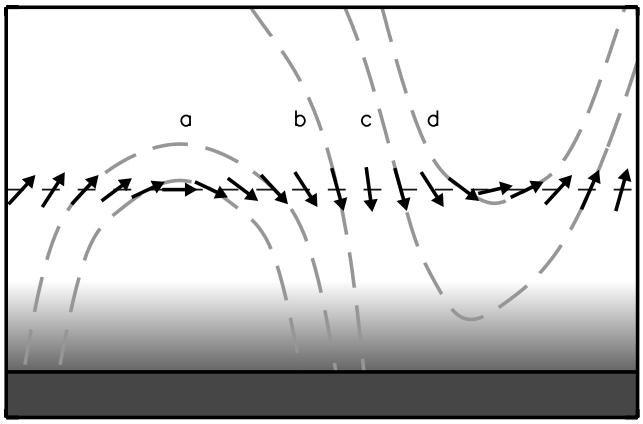

Figure 1. Possible magnetic field topologies. The Mars Global Surveyor Magnetometer and Electron Reflectometer (MGS MAG/ER) measures the local vector magnetic field near 400 km altitudes (arrows). Electron pitch angle distributions can be used to help identify whether the field angle is closed (curve a), open (curve b) or draped (curve c) in the ionosphere/atmosphere, or draped above the ionosphere/atmosphere (curve d).

for understanding the state and evolution of the Martian upper atmosphere. The field topology can be expected to constantly vary as crustal fields rotate with the planet and reconnect with the highly variable IMF.

[4] Magnetic topology can be difficult to determine unambiguously using in situ magnetometer measurements. In global simulations the magnetic field is calculated for all locations at a given instant, and the topology of a given field line can be determined directly by carefully tracing the field lines in the model [e.g., *Stern and Alexeev*, 1988; *Willis et al.*, 1997]. With measurements, however, the field is typically known only at the location of the spacecraft. In some instances reasonable assumptions can be made about the topology of a field line using only the orientation of the ambient field. For example, radially oriented field lines measured above one of Earth's polar caps are more likely to have an open topology than horizontally oriented field lines at low altitude above Earth's equator. More often, however, the characteristics of the plasma populating the flux tube are used in conjunction with any available magnetic field information.

[5] Efforts to study the Martian field topology and its effects have used each of the methods described above. Early efforts to describe the global field topology utilized vacuum superpositions of separate magnetic field models for the crustal magnetic fields and the draped IMF. Superposition of an equivalent dipole layer model by *Purucker et al.* [2000] with an MHD model for the Martian magnetosheath demonstrated that the position of the crustal sources with respect to the Sun influences the morphology of the inner magnetosheath [*Luhmann et al.*, 2002]. A similar effort combining a spherical harmonic model by *Cain et al.* [2003] with both uniform external fields and a gasdynamic model for the draped IMF suggested that the amount of magnetic flux having a given topology is sensitive to a number of factors, including the orientation of Mars with respect to the solar wind, and the orientation and strength of the IMF [*Brain*, 2002]. More recently, field lines have been traced in self-consistent simulations of the Martian solar wind interaction. A global MHD simulation showed closed field lines on the nightside [*Ma et al.*, 2002, 2004], and test particles traced in this model demonstrate how photoelectrons from the Martian dayside might travel along field lines and be observed in the induced magnetotail [*Liemohn et al.*, 2006]. In addition, a Hall-MHD simulation shows differences in topology depending upon the orientation of the strong crustal fields with respect to the solar wind and IMF [*Harnett and Winglee*, 2005].

[6] A few groups have investigated field topology at Mars using spacecraft data. These studies have largely focused on data returned from the Mars Global Surveyor Magnetometer and Electron Reflectometer (MGS MAG/ER), since MGS is the only spacecraft to make magnetometer measurements at Mars since the discovery of crustal magnetic fields. *Krymskii et al.* [2002] compared maps of the average nightside field orientation at the ~400 km MGS mapping altitude to simple dipole crustal field sources to identify likely locations of open and closed field lines. They found that the orientation of the local magnetic field does not necessarily provide a reliable indication of its topology, and that regions of radial (horizontal) magnetic field with respect to the planetary surface can sometimes be associated with closed (open) field lines. The electron energy spectrum was used by *Mitchell et al.* [2001a] to identify closed field lines on the Martian nightside. Observations for which the measured electron fluxes were consistent with instrumental background, termed "plasma voids," were inferred to be made on closed field lines in darkness where electron source processes are negligible, and have also been detected and associated with crustal fields in Mars Express electron observations [*Soobiah et al.*, 2006]. Plasma voids are punctuated in MGS data by "flux spikes" observed on radially oriented crustal field lines, where electron fluxes exceed those observed on the nightside far from crustal fields. Flux spikes were taken as indicators of open magnetic field lines. The boundary between open and closed field lines has been indirectly inferred from Mars Express radar observations, which show reflection of radio waves from tilted ionization layers adjacent to regions of radial crustal magnetic field [*Gurnett et al.*, 2005; *Nielsen et al.*, 2007].

[7] Another method for determining topology using observations involves the examination of charged particle directional information in the form of pitch angle distributions. The distribution of charged particle flux with respect to the local direction of the magnetic field might be used to infer when a given field line is connected to a source population, or when it is connected to a particle sink. Pitch angle distributions (PADs) are commonly used to determine when field lines in the solar wind are connected to the Sun [e.g., *Kahler et al.*, 1996], and to determine the topology of magnetic field lines near Earth [e.g., *Mitchell et al.*, 1987]. The objective of this paper is to present the results of an investigation of 63 million PADs measured by MGS near Mars, and to use the PADs to identify probable regions of open and closed magnetic field on the Martian nightside and on the dayside. In section 2 we describe the method used to associate the PADs with different field topologies. In section 3 we apply the method to study a single orbit on the

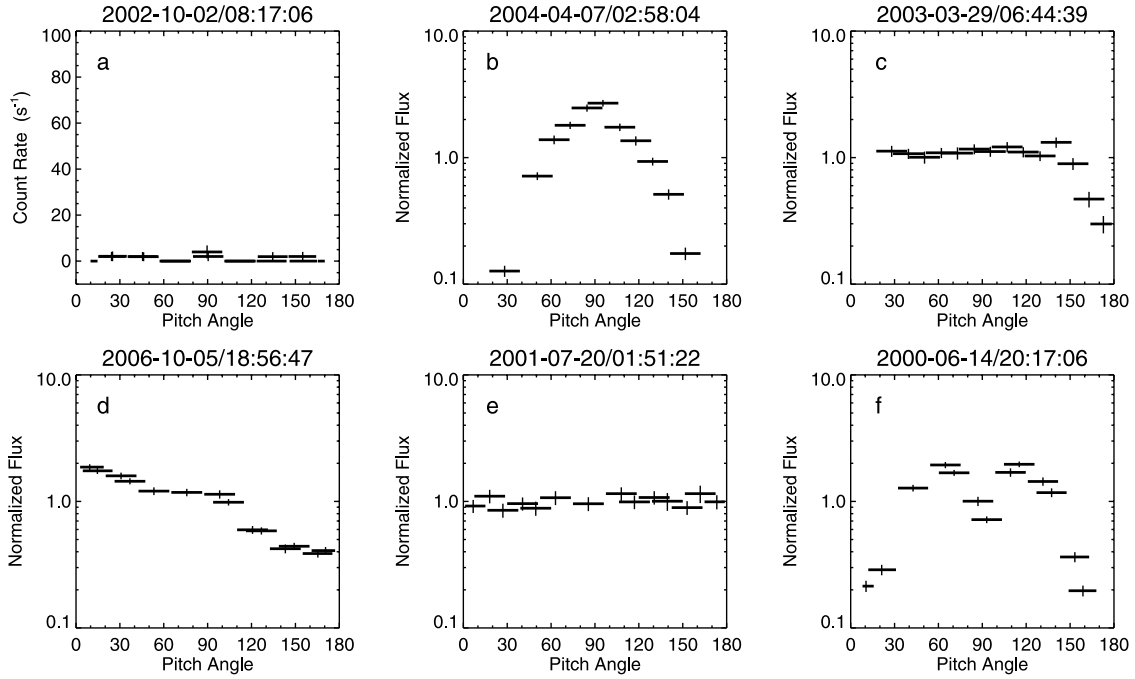

Figure 2. Representative pitch angle distributions from MGS MAG/ER: (a) plasma void, (b) two-sided loss cone, (c) one-sided loss cone, (d) field-aligned beam and loss cone, (e) flat, and (f) two-sided conic.

nightside, and to 6 years of nightside measurements to identify the frequency with which different types of PADs are observed as a function of location and magnetic elevation angle. In section 4 we apply the method to MGS dayside observations. In section 5 we summarize our results, discuss the questions left unanswered by our analysis, and identify possible future improvements and investigations of field topology near Mars.

2. Data and Method

[8] The MGS ER was a top hat electrostatic analyzer that measured superthermal electron angular distributions near Mars in energy channels ranging from 10 eV to 20 keV [*Acuña et al.*, 1992; *Mitchell et al.*, 2001a]. Directional information is available in a 14° thick plane divided into 16 sectors measuring 22.5° wide. Coupled with vector magnetic field data recorded by MAG, a 2-D slice through the pitch angle distribution was collected every 2–8 s. The MGS spacecraft was three-axis stabilized (did not spin), so full 3-D distributions are not available. Further, the 2-D PAD has variable width since the orientation of the ambient field with respect to ER varies. For example, at times when the field direction was in the plane of the instrument field of view all 180° of pitch angle space were sampled. At times when the field direction was nearly perpendicular to the field of view only pitch angles near 90° were sampled. Since the field of view of the instrument covers 360°, most of the measured PAD was sampled by two different sectors of ER. For example, in the event that the ambient field lies in the center of the FOV of one of the instrument sectors, one can see that the sectors immediately adjacent to this central sector both sample the same range of pitch angles.

[9] In this work we analyze PADs recorded from 1 July 1999 to 2 November 2006, while MGS was in its mapping orbit. The orbit was nearly circular with altitude of 405 ± 36 km, and maintained at a local time of ~2 A.M./2 P.M. The orbit period was 1.96 hours, so that successive orbit tracks projected onto the surface are 28° apart. At 400 km the strongest crustal fields are 220 nT, and have size scale of hundreds of kilometers [*Connerney et al.*, 2001]. External fields at mapping altitude are typically 35 nT at low solar zenith angles (SZA) and 10 nT at high SZA [*Brain et al.*, 2003].

[10] ER records PADs in 19 energy channels, but only a few channels are appropriate for our analysis. The flux of electrons at high energies (>500 eV) is usually too low to reliably determine the shape of the PAD. In low-energy channels (<100 eV) the variable spacecraft potential and intermittent secondary electrons generated at the spacecraft through photoionization or particle impact complicate determination of the angular distribution of ambient electrons with a given energy. Also, an attenuator is used for energy channels lower than 95 eV to prevent the instrument from saturating at low energies; as a result the signal-to-noise of the PADs at energies of ~60–100 eV can be too low for our present analysis. We have chosen data from the energy channel centered at 115 eV (95–148 eV).

[11] Our approach in this analysis will be to use the shape of the observed pitch angle distributions to infer the topology of the flux tube MGS occupies during each observation. Several representative PADs are shown in Figure 2, each with a different shape. To show how topology might affect the observations, let us first consider the motion of electrons near Mars along field lines of different topology. The possible field topologies are shown in Figure 1. Electrons in motion along these field lines may adiabatically change their pitch angle in regions of converging or diverging magnetic field and may also be absorbed (recombine or thermalize) in the collisionally thick

atmosphere. Additionally, new electrons may be added to the distribution via source processes. The use of PADs to identify field topology is made considerably more difficult in situations where electron source processes are nonnegligible. The largest source of superthermal electrons at Mars comes from photoionization of upper atmospheric neutrals, resulting in addition of planetary photoelectrons to the shocked solar wind electron population. This process only operates in sunlight, so we confine ourselves in the discussion below to field lines that are in darkness at low altitudes (where photoionization is significant).

[12] Closed magnetic field lines (labeled "a" in Figure 1) intersect the Martian crust at both ends. As electrons in a closed flux tube move from high to low altitude they encounter regions of increasing field strength, and should adiabatically mirror (reverse the direction of their velocity along the field line), bouncing back and forth along the field line. The altitude of the mirror point for a given electron measured at the spacecraft is controlled by its pitch angle; more field aligned electrons (pitch angles close to 0° or 180°) will mirror at lower altitudes than those with pitch angle near 90°. Those electrons with sufficiently low mirror point will collide with the atmosphere before they are able to reflect, and be lost from the distribution. In the absence of electron sources one might expect to measure a pitch angle distribution similar to the one shown in Figure 2b, with fewer field aligned electrons than at pitch angle of 90°. These two-sided loss cones are not sharply defined as they are at the Moon [*Halekas et al.*, 2001], since as the pitch angle of an electron incident upon the atmosphere becomes less field aligned its reflection altitude becomes higher and therefore the column of absorbing atmosphere it encounters becomes smaller. The Martian atmosphere absorbs electrons less efficiently as their pitch angle becomes less field aligned (R. J. Lillis et al., Electron reflectometry in the Martian atmosphere, submitted to *Icarus*, 2007, hereinafter referred to as Lillis et al., submitted manuscript, 2007). In reality, some fraction of electrons interacting with the atmosphere will backscatter via collisions before they can be absorbed and will remain in the distribution, in some cases modifying the location of the loss cone by as much as 10° [*Lillis et al.*, 2004]. Since both ends of a closed field line are anchored in the atmosphere, backscattered electrons should to first order contribute equally to both sides of the observed PAD. As an extreme example of the situation in Figure 2b one might expect to observe very few electrons at all pitch angles (Figure 2a), if all electrons on a field line are absorbed by the atmosphere or otherwise removed from the flux tube. Plasma voids were reported in MGS data by *Mitchell et al.* [2001a].

[13] Open field lines (labeled "b" in Figure 1) intersect the crust at only one end, allowing particle exchange between the solar wind and the Martian atmosphere. An electron traveling toward the planet along the field line will be absorbed by the atmosphere at low altitudes (160–230 km), unless the field converges sufficiently to cause it to mirror. In the presence of converging fields (i.e., on crustal field lines) the most field-aligned incident electrons will be absorbed, while those with pitch angles close to 90° will mirror. A depletion in the field-aligned flux returning from the atmosphere will form (Figure 2c), analogous to the two-sided loss cone described above. One-sided loss cones on the Martian nightside have been analyzed and modeled in MGS data in order to determine magnetic field strength at the exobase and neutral atmospheric densities [*Lillis et al.*, 2004, 2005].

[14] Draped field lines do not intersect the Martian crust anywhere; they are entirely associated with the IMF draped around the conducting dayside ionosphere and stretched into an induced magnetotail at night. If a draped field line does not encounter the collisional atmosphere (labeled "d" in Figure 1) then the observed PAD will be that associated with the shocked solar wind at Mars. If a draped field line is embedded in the collisional atmosphere (labeled "c" in Figure 1), then the solar wind has access to the spacecraft from only one direction along the field line. Incident electrons of all pitch angles should be absorbed in the absence of converging fields, and the return flux (which could be as high as 20% of the incident flux) should consist entirely of backscattered electrons (Figure 2d). In a very few cases where the field line only grazes the top of the collisional atmosphere, some solar wind electrons from the distant field line can be expected to reach the spacecraft from below as well.

[15] Note that for field lines labeled both "b" and "c" in Figure 1 the expected PADs at 400 km are quite similar, with identical incident distributions, and a return flux consisting mostly of reflected and backscattered electrons. It is rather difficult to distinguish these two types of field lines from each other based on observations of PAD shape. For the purposes of this paper we consider the collisional atmosphere to be the reference surface for the determination of topology, so that field lines are "open" or "closed" with respect to the atmosphere and not the planetary surface. Further, it can be difficult to distinguish between draped field lines that intersect the atmosphere and those that do not since the solar wind distribution is very often anisotropic. Where possible, we rely on context (in the form of geographic location or electron energy distributions) to distinguish between field lines of types b–d in Figure 1. Future investigations may seek to distinguish these types of field lines, perhaps using a modification of the method of *Lillis et al.* [2004] based on the precise shape of the loss cone in the upward electron flux.

[16] The variety of pitch angle distributions resulting from the different topologies described above are distinguished from each other according to their shape. For each observation we resample the data from the 16 instrument sectors into 128 equal-sized pitch angle bins spanning 180°, after first background subtracting the distribution and ignoring data from two instrument sectors that have been determined through on-orbit calibration to have high noise levels. Each half of a PAD is then taken separately (0°–90° and 90°–180°) and the flux at 90° pitch angle is compared to the most field-aligned flux for the observation. Observations are separated according to whether the flux at 90° pitch angle exceeds the field-aligned flux by more than 2.58σ ("loss cone"), whether the field-aligned flux exceeds that at 90° by more than 2.58σ ("field-aligned beam"), or whether the two fluxes are within 2.58σ of each other ("isotropic"). In addition, we identify observations for which the flux at an intermediate pitch angle exceeds or is exceeded by the flux at 90° by more than 2.58σ ("conic," "inverse conic"). In this manner, all usable PADs measured

by MGS are processed and assigned to two categories (one for each half of the distribution) based on shape.

[17] More than 63 million PADS, recorded over a period of 7 years by ER, form the basis of this study. A number of observations were excluded for different reasons. A few (0.5%) are excluded because of instrument saturation during periods of high electron flux. This can occur on the dayside during periods of high solar wind pressure [*Brain et al.*, 2005] and on the nightside during auroral-like electron events [*Brain et al.*, 2006]. Some PADs (4%, mostly on the nightside) have count rates that were statistically zero across all instrument sectors. They are classified as ''plasma voids'' for further study, but their shape is not classified as described in the paragraph above. A relatively large number of observations (34%) are rejected because of uncertainty in the pitch angle mapping, resulting from uncertainty in the ambient field direction. We remove all data for which this uncertainty exceeds 15°, corresponding to field magnitudes of less than 12 nT. This criterion removes a significant fraction of data on the nightside far from strong crustal fields, but is required to ensure that the resampling of data from the 16 sectors (measuring 22.5°) into discrete pitch angle bins is accurate. Finally, we exclude all data for which the width of the measured PAD is smaller than 90° (21%). PAD data that are not fully sampled across the distribution may not capture features in the field-aligned electron flux crucial to the determination of topology. However, MAG/ER seldom sampled a full 180° distribution. We experimented with different thresholds for the acceptable PAD width, and found that use of all distributions with >90° width provides results that agree with more selective thresholds while reducing statistical uncertainty. This criterion results in the systematic exclusion of a large fraction of observations in some locations above crustal fields, where the orientation of the local field always provides a narrow distribution. In all, 43% of the available observations meet our selection criteria (including plasma voids).

[18] We identify 27 different types of PADs in MAG/ER data. These include unusable data (saturated, high field direction uncertainty, narrow PAD), plasma voids, and 25 PAD types classified according to the shapes of the incident and return distributions, determined independently. There are 5 different types of incident or downward traveling distribution (isotropic, loss cone, field-aligned beam, conic, inverse conic) and 5 different types of return or upward traveling distribution. Figure 2 shows several examples measured by MGS, some of which have already been described above. In all examples the ambient magnetic field had negative radial component, so that pitch angles 0°–90° correspond to incident electrons and 90°–180° correspond to return electrons. All examples were also chosen from times when the PAD width exceeded 160°. Figure 2a shows a typical plasma void, with statistically insignificant count rates in all instrument sectors. Figures 2b–2f show normalized fluxes for five characteristic PAD types, including a two-sided loss cone, a loss cone in the return flux, a field-aligned beam in the incident flux with loss cone in the return flux, an isotropic distribution, and a two-sided conic. All 27 PAD types have been mapped as a function of geographic location and ambient field. The results of this effort are described in the following sections.

[19] Before proceeding, we also verify that 115 eV electrons can provide appropriate information about field line topology. Electrons with energy of 115 eV have velocity of ~6400 km/s, so can travel distances equivalent to several times the radius of Mars in a typical ER integration of 2–8 s. Therefore the two sides of the PAD can be considered to be representative of a single field line that stretches as much as 10,000 km or more. Calculated cross-field drifts are relatively small (<10 km/s), so electrons can reasonably be associated with a single flux tube (Lillis et al., submitted manuscript, 2007). We assume that all distributions are gyrotropic and that the effects of electric fields on the distributions are negligible.

3. Nightside Topology

[20] We first consider topology of field lines measured by MGS when it was in eclipse on the nightside of Mars. Photoionization of atmospheric neutrals is less likely to occur on field lines sampled by MGS when it is in darkness, so that the measured PADs contain fewer signatures of local electron source populations which can complicate determination of topology. However, we are mindful that even when MGS is in darkness the flux tube it samples may have sunlit portions at distant locations, and therefore may contain photoelectrons [e.g., *Frahm et al.*, 2006; *Liemohn et al.*, 2006]. At 400 km altitudes MGS enters eclipse at solar zenith angle of ~120°.

3.1. Case Study

[21] The nightside portion of an example MGS orbit from 15 November 2000 is shown in Figure 3. A number of PAD types are observed over the course of the orbit as MGS travels southward from a region lacking significant crustal fields and encounters several moderately strong sources. From 2026 until 2042 (labeled ''1'' in Figure 3) the electron flux is lower for pitch angles near 180° than at 90° during a time when the ambient field is oriented radially downward toward the planet. These loss cones indicate the absorption of incident electrons below the spacecraft, and we conclude that the flux tubes that MGS occupies during this time intersect the atmosphere. However, the topology of these field lines could be either open or draped. Notice that the normalized flux from 0°–90° pitch angle changes near 2035, as MGS moves into a region where the crustal field strength begins to increase and become more radial. Prior to 2035 there is a relatively sharp contrast between the downward and upward halves of the PAD, and the loss cone forms relatively close to 90°. Several of the incident PADs during this time are identified as field-aligned beams by our algorithm. After 2035, on the fringes of a crustal field, there is no such contrast between incident and return fluxes, and the loss cone forms at more field-aligned pitch angles. We interpret this change in the PADs as a transition by MGS from nonconverging draped field lines (that likely intersect the atmosphere) to converging open field lines that intersect the crust.

[22] After 2040 MGS passes through a region of crustal fields. The omnidirectional electron flux in this region is more variable than in the northern hemisphere, and can vary by orders of magnitude depending upon the location. The width of the pitch angle distribution varies considerably as

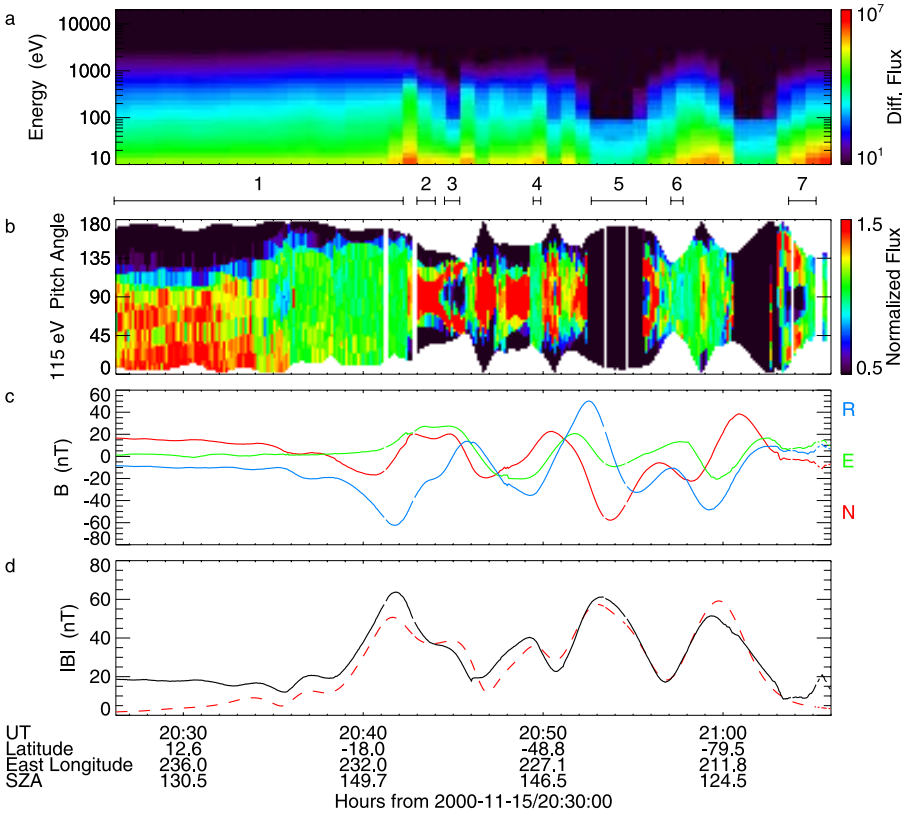

Figure 3. Nightside MGS pass on 15 November 2000. (a) Omnidirectional differential electron flux measured by ER (number of electrons/(cm^2 s sr eV). (b) Normalized pitch angle distributions measured by ER. (c) Vector magnetic field measured by MAG, with northward (blue), eastward (green), and radial (red) components. (d) Field magnitude measured by MAG (black) and predicted using the spherical harmonic model of *Cain et al.* [2003] (dashed red). Figure 3a has lower time resolution than Figure 3b. Numbered time periods are discussed in text.

the relative orientation of the crustal fields and the spacecraft change. Two-sided loss cones are evident from 2033 to 2044 (labeled "2" in Figure 3), indicating closed crustal magnetic field lines in a region where the local field is within 33°–46° of horizontal. Several other periods of trapped distributions on closed field lines are evident in Figure 3.

[23] Conic distributions of electrons are evident from 2044:30 to 2045:20 (labeled "3" in Figure 3), and resemble trapped distributions that have been depleted in electrons at 90° pitch angle. First observed at Earth [*Menietti and Burch*, 1985], electron conics may form by a variety of mechanisms ranging from simple combination of field-aligned beam and loss cone distributions to time-variable parallel electric fields and heating by a variety of wave mechanisms (see discussion of *Eliasson et al.* [1996]). Electron conics are associated with Earth's polar caps and auroral zone and are often associated with upward ion beams or conics. Distributions of this type are often seen in MGS nightside observations in crustal field regions, and will be presented in more detail in a separate study. They are seen again in Figure 3 at 2055:30–2056.

[24] In a few places the PADs are statistically isotropic, most notably at 2049 (labeled "4" in Figure 3) and at two time periods from 2057:30–2100. In all three cases, wider PADs from nearby time periods show evidence for one- or two-sided loss cones, suggesting that an isotropic distribution observed in darkness by MGS on the nightside is likely not to be isotropic at pitch angles left unsampled by MGS. Isotropic PADs could be either open or closed, depending upon whether there is a depletion on both sides of the unsampled portion of the full distribution.

[25] Plasma voids are also evident in the pass shown in Figure 3. In the region labeled "5" the omnidirectional fluxes are very close to instrumental background (the energy spectra in Figure 3 have not been background subtracted, and the attenuator used for energies <100 eV creates a greater background than for higher energies). The corresponding normalized PADs have been set to zero for display purposes. Another similar region is evident from 2100:30–2102:30. Trapped and conic distributions are observed in regions surrounding the voids, consistent with the idea that these are closed field lines.

[26] A few periods were excluded from our analyses. Observations in the region labeled "6" were recorded during a time when the PAD width was smaller than 90°, making it very unlikely that we can successfully determine the shape of the full distribution. Another similar period occurred between 2045 and 2046, where the conics in the preceding PADs likely move to pitch angles outside of the sampled range, and the location of the loss cones in the subsequent distributions is also outside of the sampled

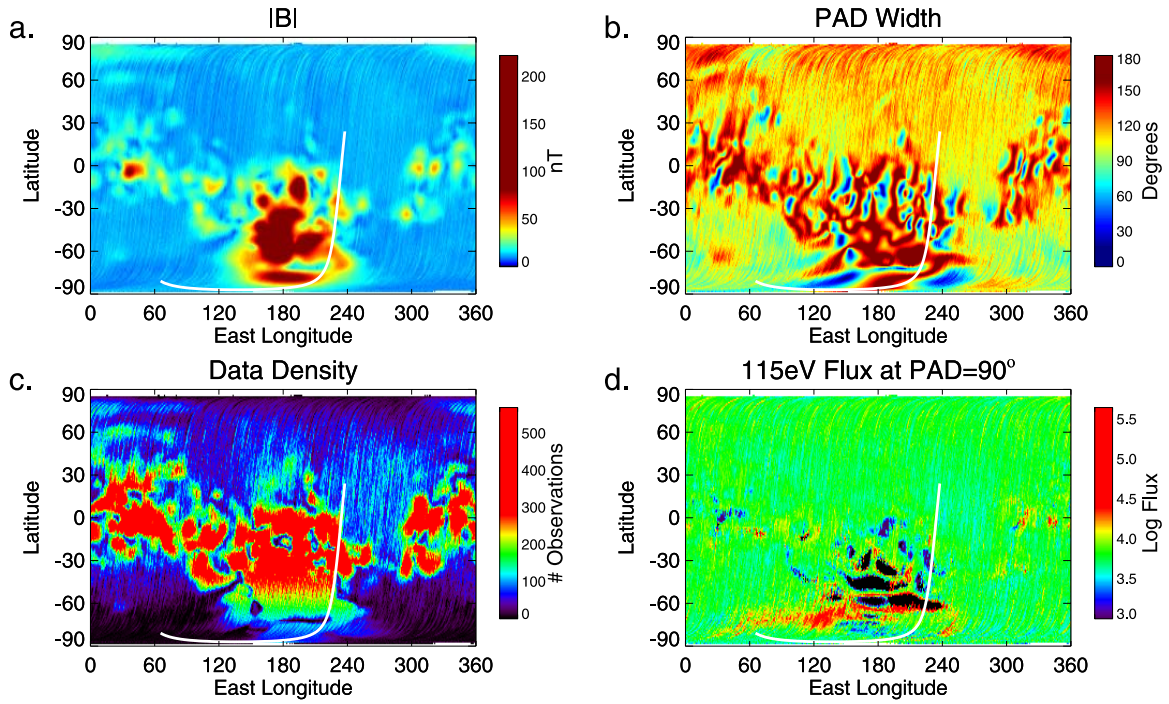

Figure 4. Nightside environment for MGS electron measurements as a function of geographic location averaged in 1° × 1° bins. (a) Average magnetic field magnitude. (b) Average pitch angle distribution width. (c) Usable data coverage. (d) Differential 115 eV electron flux (number of electrons/(cm^2 s sr eV) at 90° pitch angle. The spacecraft trajectory for the pass in Figure 3 is overplotted in each panel.

range. Observations in the region labeled "7" occurred during a period of low magnetic field amplitude, and corresponding high uncertainty in the pitch angle range for each of the instrument sectors. Even though several of these observations had a wide PAD and appear to have clear pitch angle signatures, we conservatively exclude them.

[27] In addition to the electron signatures of topology, Figure 3 also shows interesting small-scale features in the magnetic field that merit future study. For example, discontinuities in the field amplitude and vector components are observed in five or six different locations in the crustal field regions. Field discontinuities can be caused by current-generated magnetic fields, and one example has been previously reported in a cusp of crustal magnetic field during a period of auroral-like electron acceleration [*Brain et al.*, 2006]. Currents are likely to form at topological boundaries and near the locations of pressure gradients in the plasma. Some weak magnetic oscillations are also apparent toward the end of the orbit pass; magnetic oscillations at the local ion gyrofrequency have been reported on the Martian nightside by *Espley et al.* [2004, 2005], and may provide insight into the formation of electron distributions near Mars and plasma acceleration mechanisms.

3.2. Statistical Results

[28] Over a period of several years MGS passed hundreds of times over most parts of the Martian surface at the same altitude. We have categorized the PADs from 7 years of observations in order to learn the dominant distribution shape observed above each location. Details of the magnetic and plasma environment in which angular distributions are recorded on the nightside are shown in Figure 4. The strongest crustal magnetic fields are clustered in one region of the southern hemisphere (Figure 4a), and moderate crustal fields are observed near the equator and in one part of the northern hemisphere [*Acuña et al.*, 1999]. The field magnitude at 400 km in other locations is typically on the order of 10 nT. The average PAD width recorded by MGS (Figure 4b) varies considerably as a function of geographic location. Above strong crustal fields the PAD width is relatively constant from orbit to orbit, since the relative orientation of the ambient field and the ER field of view is constant. This leads to some regions where the PAD is nearly always very narrow, and other regions where it is nearly always very wide. Far from crustal fields (e.g., in the northern hemisphere) the average PAD is usually greater than 100°, but has greater orbit-to-orbit variability since the ambient field is dominated by the draped IMF, which constantly changes its orientation. The population of usable PADs (Figure 4c), including plasma voids, shows that many data were excluded in regions where the field strength is low or the PAD is too narrow. In some locations at high southern latitudes there are fewer than 20 usable PADs in each 1° × 1° geographic bin. In other locations near crustal fields there are more than 500 PADs per bin.

[29] Regardless of the width of the distribution or the strength of the local magnetic field, it is nearly always possible to determine the flux of electrons at 90° pitch angle using MAG. The average flux (taken as a geometric mean) as a function of location, shown in Figure 4d, is 5000–10,000 cm^{-2} (s sr eV)$^{-1}$ at 400 km altitudes over most of the surface on the nightside. Above moderate and strong crustal fields, however, it can be much lower (statistically zero in some locations) or much higher. Above the region

Table 1. Percentage of Usable Distributions Associated With Each PAD Type When MGS Was in Eclipse[a]

	Incident Distribution				
Return Distribution	Isotropic	Loss Cone	Field-Aligned Beam	Conic	Inverse Conic
Isotropic	8.8	1.1	3.4	0.3	0.1
Loss cone	23.1	12.8	7.5	0.4	0.4
Field-aligned beam	0.6	0.2	2.8	0.2	0.0
Conic	0.8	0.3	3.9	1.4	0.0
Inverse conic	0.0	0.1	0.1	0.0	0.0

[a]Incident and return PAD types are defined in text. Plasma void is 31.5% All values are given as percentages.

centered near (160° E, 70° S), in particular, the average flux is as high as 40,000/(cm^2 s sr eV), higher than for any region at the same altitude on the dayside. High average electron fluxes at 115 eV likely result from the considerable number of peaked auroral-like electron distributions in this location reported by *Brain et al.* [2006]. Auroral-like energy spectra and the detection of low-altitude current sheets [*Halekas et al.*, 2006] suggest an electron acceleration process is active in this region, resulting in enhanced fluxes. Times of especially high 115 eV electron flux, when the ER instrument saturated, are not included in this analysis so that values shown in Figure 4 should be taken as lower bounds to the average flux in each region.

[30] The results of a statistical analysis of all usable nightside ER PADs, including plasma voids, are summarized in Table 1. More than 95% of the distributions can be classified as one of 10 types. MGS spends nearly 1/3 of the time while in eclipse in flux tubes void of plasma, where no 115 eV electrons are discernible. Field-aligned beams and isotropic distributions are both detected more often in the incident flux than in the return flux, while loss cones and conics are observed more often in the return flux than the incident. Inverse conics are rarely identified, as expected since we lack a physical interpretation for such a distribution. The incident distribution is a field-aligned beam 20% of the time, and isotropic more than 30% of the time. The return distribution is a loss cone 44% of the time, and a conic 7% of the time. Recall from Figure 3, however, that isotropic PADs may often be observations for which the width of the measured distribution was too narrow to distinguish field-aligned features such as loss cones or beams. Indeed, as the PAD width threshold is made stricter, the percentage of isotropic distributions decreases, and the percentage of source and loss cones increase.

[31] The nightside geographic distribution of several PAD types is shown in Figure 5. Plasma voids (Figure 5a) are concentrated near crustal magnetic fields, as shown by *Mitchell et al.* [2001a]. Near the strongest crustal fields 100% of the measurements in some locations can be classified as plasma void, meaning that in no time during the 7 years of observation was a statistically significant flux of electrons present on the flux tubes MGS sampled at 2 A.M. local time. We infer that the field lines in these regions are always closed, regardless of external conditions. Plasma voids are also observed less often in regions of weaker crustal magnetic field, indicating some variability in the structure and topology sampled by MGS above these regions. Very few voids (0–10%) are seen at large distances from crustal magnetic fields, indicating that loops of closed field connecting crustal fields in widely separated locations either do not exist on the nightside or contain significant electron fluxes.

[32] Two-sided loss cones (Figure 5b) are detected 30–50% as often as plasma voids on the nightside, but are distributed over a larger range of locations. They are most commonly observed near crustal fields, and are most concentrated in regions surrounding plasma void locations. We interpret these PADs as trapped distributions on closed field lines. Trapped distributions are nearly always evident near (160° E, 70° S), where high electron fluxes (Figure 4d), auroral-like energy spectra [*Brain et al.*, 2006], and current sheets [*Halekas et al.*, 2006] are also often seen.

[33] Figures 5a and 5b together suggest that the outer layers of a region of closed magnetic field contain electrons while the inner layers do not. Electron loss processes must dominate source processes in the inner layers for voids to be observed. If we assume source processes have been negligible since these field lines were last in sunlight, then any electrons that populated these field lines have been lost in the preceding 6–8 hours. Many of these electrons are absorbed by the atmosphere within fractions of a second. Electrons with pitch angles near 90°, however, do not have trajectories that intersect the atmosphere. They must either be scattered in energy or into more field-aligned pitch angle trajectories (possibly through wave interactions), or must diffuse outward. While all of these processes may act to form plasma voids, we do not favor the latter explanation for the presence of trapped distributions in the outer layers, since it requires that the timescale for outward diffusion be very similar to the amount of time the field lines have been in darkness, regardless of the size or strength of the crustal fields. The trapped electrons, then, have populated the closed field lines more recently. This could occur via recent (less than the timescale for scattering or diffusion) magnetic reconnection of an open field line containing superthermal electrons, or via inward cross-field diffusion from surrounding regions.

[34] Figures 5d and 5e show the locations of PAD distributions that have a depletion (loss cone) in the upward flux, and the incident fluxes are consistent with either isotropic distributions or field-aligned beams. These distributions are often seen above the weakly or nonmagnetized northern plains, and in some locations near crustal magnetic fields. We interpret many of these observations as occurring on field lines that are connected at one end to the draped IMF, and at the other to the atmosphere. However, upward loss cones can be indicative of both open and draped field lines, as discussed in section 3.1, and both are certainly represented in Figures 5d and 5e. Incident field-aligned beams and isotropic distributions are observed a similar percentage of the time above unmagnetized regions. However, incident isotropic distributions are far more likely than field-aligned beams near crustal fields, which can be explained by adiabatic modification of incident beamed distributions in converging crustal magnetic fields, so that the PAD is isotropic by the time it reached MGS at 400 km altitudes.

[35] To highlight the geographic differences in the distributions represented in Figures 5d and 5e, we calculated

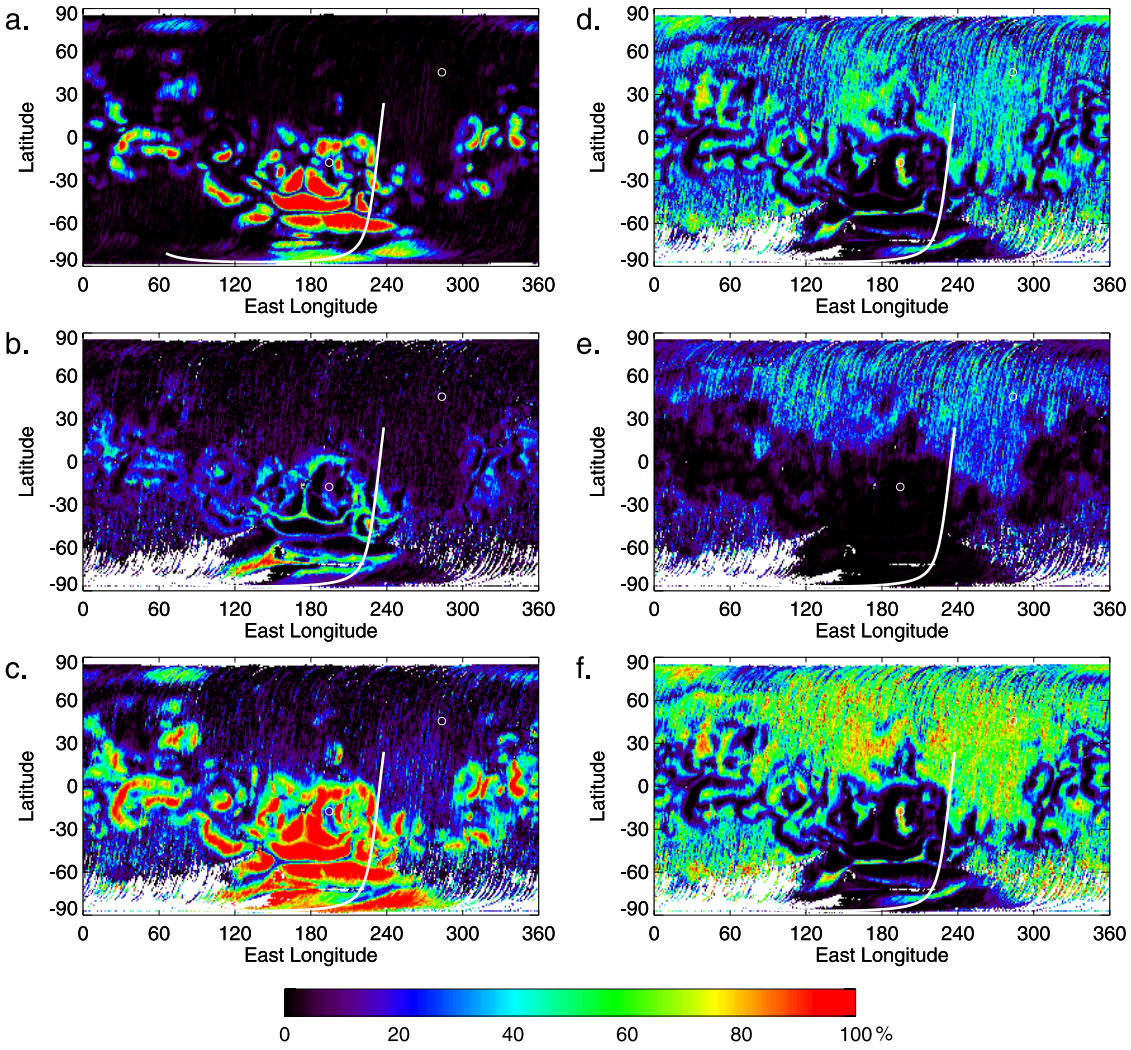

Figure 5. Frequency of occurrence of different pitch angle distribution types on the Martian nightside as a function of geographic location: (a) plasma voids, (b) two-sided loss cones, (c) superposition of Figures 5a and 5b, (d) incident isotropic with returning one-sided loss cone, (e) incident field-aligned beam with returning one-sided loss cone, and (f) superposition of Figures 5e and 5f. Frequencies in $1^\circ \times 1^\circ$ bins containing fewer than 10 independent usable measurements are not shown. The spacecraft trajectory for the pass in Figure 3 is overplotted in each panel, and the locations for the mean PADs in Figure 5 are indicated by white curves.

the mean PAD for all observations represented in Figures 5d and 5e from two $1^\circ \times 1^\circ$ regions. Figure 6a shows that the PADs above a strong crustal field region have a more sharply defined loss cone and are more repeatable than the PADs above a region lacking crustal fields. The field magnitude above the crustal field is ~123 nT, creating an isotropic incident flux at 400 km, regardless of whether the flux at higher altitudes (and lower field strength) is beamed. The loss cone forms near 140° in a narrow range of pitch angles that is not much larger than the 22.5° width of the ER instrument sectors, indicating that the ratio of field strengths between 400 km and the absorption layer in the atmosphere does not vary much over a given location during a 6 year period. In contrast, the incident flux in the weakly magnetized region is sometimes isotropic and sometimes beamed, and the loss cone forms over a broad range of pitch angles ranging from 90–140°. This suggests that the field lines in these locations do not converge to the same degree as field lines near the crustal source. Indeed, the flux of the 1σ lower bound PAD falls steeply from 90–110°, indicating that many observations are consistent with nonconverging fields intersecting the atmosphere. Further, the change in orientation of the local field from orbit to orbit is more consistent with a draped field line configuration than one where the field line is connected to a crustal magnetic field.

[36] Figure 5c shows the likelihood of measuring either a plasma void or a two-sided loss cone above each geographic region, combining the results of Figures 5a and 5b. Similarly, Figure 5f combines the results of Figures 5d and 5e. Topologically, we believe that the measurements represented in Figure 5c are of closed field lines, while those in Figure 5f are of open or draped field lines. The two maps are quite complementary and in many locations the fields almost always have the same topology, which influences the

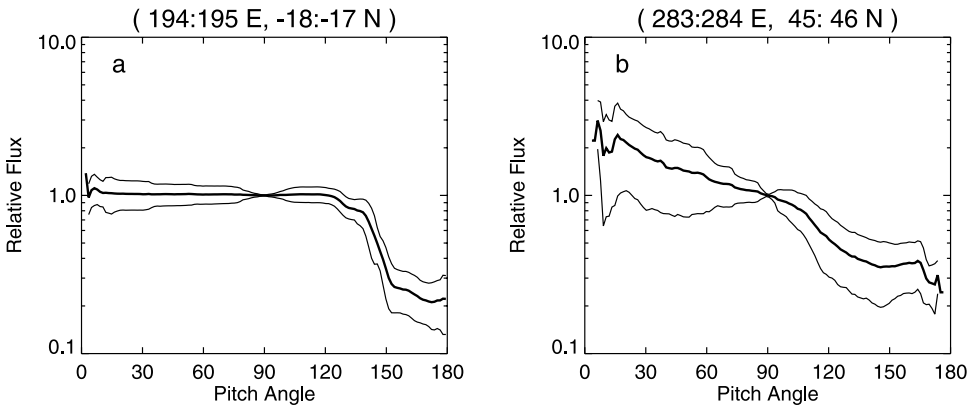

Figure 6. Mean pitch angle distributions (and standard deviation) for the observations shown in Figure 5c. (a) A location near strong crustal magnetic fields. (b) A location in the northern hemisphere far from significant crustal fields. All PADs are normalized to the flux at 90° pitch angle. PADs in Figure 6b have been reversed when necessary so that 0°–90° pitch angle corresponds to the incident flux.

expected structure of the nightside atmosphere as well as the physical processes that might be observed in different locations. Another important point is that the topology varies between open and closed in many regions. This implies that the configuration of nightside magnetic fields varies on hourly timescales, likely through magnetic reconnection. If reconnection does operate at Mars, then the convection pattern of reconnecting field lines must be complex.

[37] The results of Figure 5 suggest that the probability of MGS encountering field lines of different topology is influenced by the strength of any ambient crustal magnetic field below the spacecraft. The topology is also affected by the elevation angle of the ambient crustal field, as shown in Figure 7. As expected, closed field lines are more commonly observed when the local field is horizontal, and open/draped field lines are more common when the local field is radially oriented. Plasma voids are more common than trapped distributions at small elevation angles, and less common at large elevation angles; Figure 1 illustrates that as MGS passes through a region of closed magnetic field the outer layers (containing trapped distributions) are more likely to be vertically oriented than the interior regions. Of the distributions containing loss cones in the return flux, incident isotropic distributions are more common at high crustal field elevation angles while incident field-aligned beams are equally likely (within error) at all elevation angles greater than ~20°. These results can be explained in the context of Figures 5d and 5e. Isotropic incident distributions should be observed more often when the magnetic field diverges above the spacecraft, as it would on radially oriented crustal field lines. Elevation angle should not influence the likelihood of observation of anisotropic incident distributions observed in unmagnetized regions, since the fields in those regions should not diverge above the spacecraft to the degree that crustal fields do. If the ambient field has too small an elevation angle then the flux tube is less likely to intersect the absorption layer in the atmosphere, with the result that fewer loss cones in the return flux are observed.

[38] All geographic nightside results have been synthesized in Figure 8, which shows the dominant PAD type as a function of location at 400 km altitudes. Plasma voids and surrounding trapped distributions are common near strong and moderate crustal fields, along with regions of open field lines containing isotropic incident flux and a loss cone in the return flux. Also common near crustal fields are fully isotropic distributions; however, further inspection reveals that their measurement frequency steadily decreases as the width of the sampled distribution increases. They are more likely trapped or one-sided loss cone distributions that have not been fully sampled in pitch angle space by ER. A very few locations near crustal fields are dominated by conics. Above weakly or unmagnetized regions loss cones in the return flux dominate the observations, with the incident flux either consistent with an isotropic distribution or a field-aligned beam. The few locations colored black in Figure 8 are dominated by one of the remaining PAD types.

4. Dayside Topology

[39] We next consider pitch angle distributions recorded on the dayside of Mars, when the solar zenith angle was less

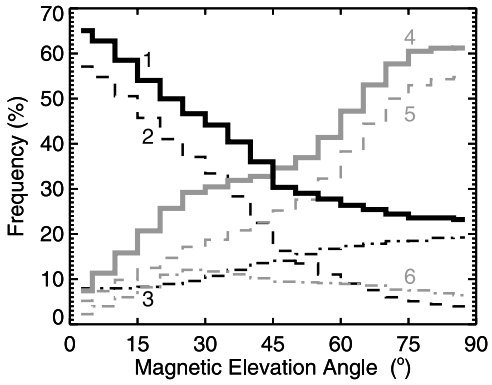

Figure 7. Frequency of occurrence of different PAD types as a function of the average magnetic elevation angle with respect to the planetary surface: 1, plasma voids and trapped distributions; 2, plasma voids; 3, trapped distributions; 4, one-sided loss cones; 5, incident isotropic, upward loss cone; and 6, incident field-aligned beam, upward loss cone.

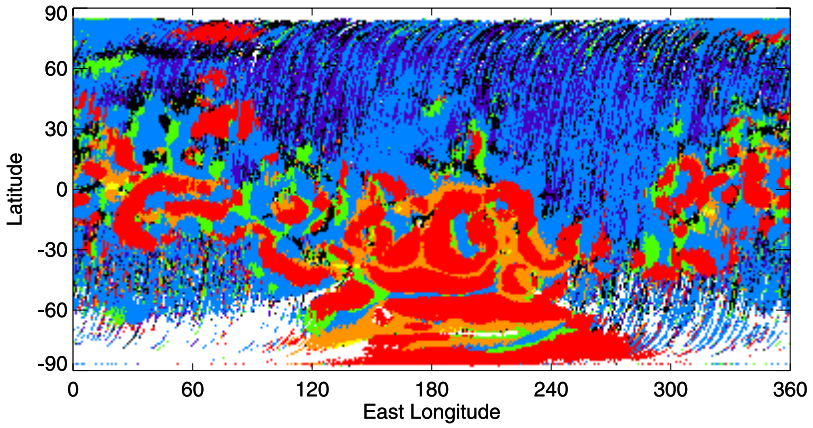

Figure 8. Geographic map of dominant PAD types recorded by MGS ER at 400 km on the nightside: plasma voids (red); trapped (orange); fully isotropic (green); incident isotropic, return loss cone (blue); incident field-aligned beam, return loss cone (purple); conic (yellow); and other (black).

than 90°. Photoionization of atmospheric neutrals is a substantial source of electrons observed on the dayside by MGS [*Mitchell et al.*, 2000, 2001a], and electron impact ionization should also occur where the shocked solar wind has access to neutrals [e.g., *Crider et al.*, 2000]. We expect therefore that electron source processes are significantly more active on the dayside than in eclipse, and that the PADs should contain the signatures of these electrons.

4.1. Case Study

[40] A dayside pass by MGS from 12 February 2002 is shown in Figure 9. MGS travels northward at 2 P.M. local time, encountering strong crustal magnetic fields at southern midlatitudes. MGS was in regions lacking significant crustal fields during the periods labeled "1" and "4" in Figure 9. During these times the radial component of the magnetic field was very small (a few nanoteslas), consistent with a field draped around the planetary solar wind obstacle. PADs during these periods show a depletion in the upward

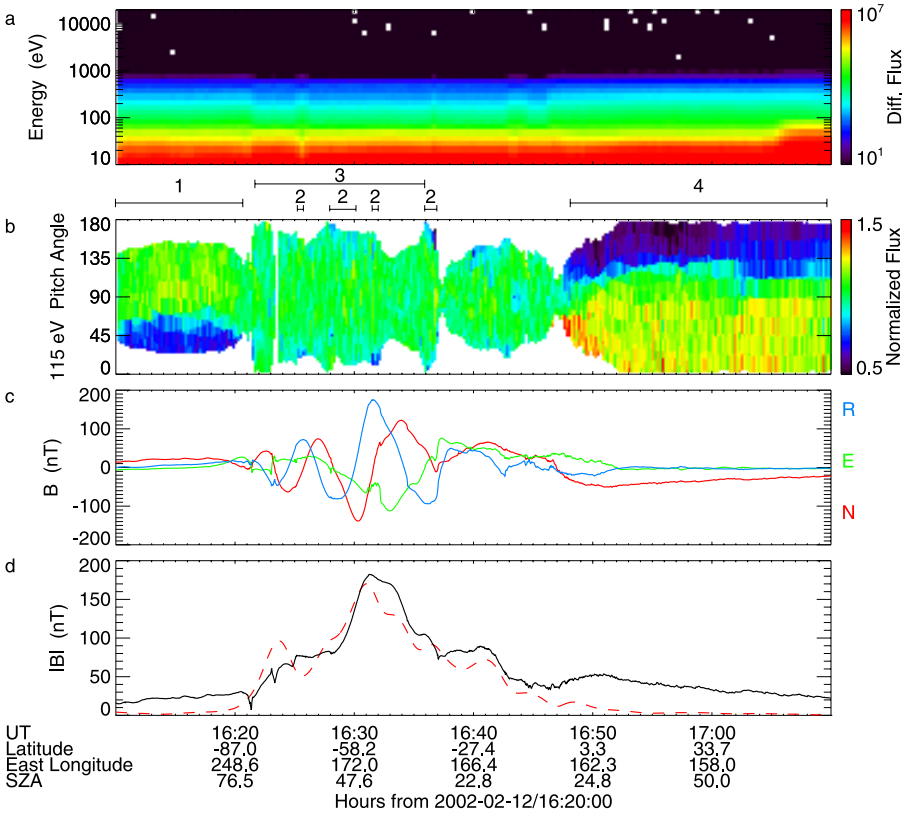

Figure 9. Dayside MGS pass on 12 February 2002, with panels analogous to Figure 3. Numbered time periods are discussed in text.

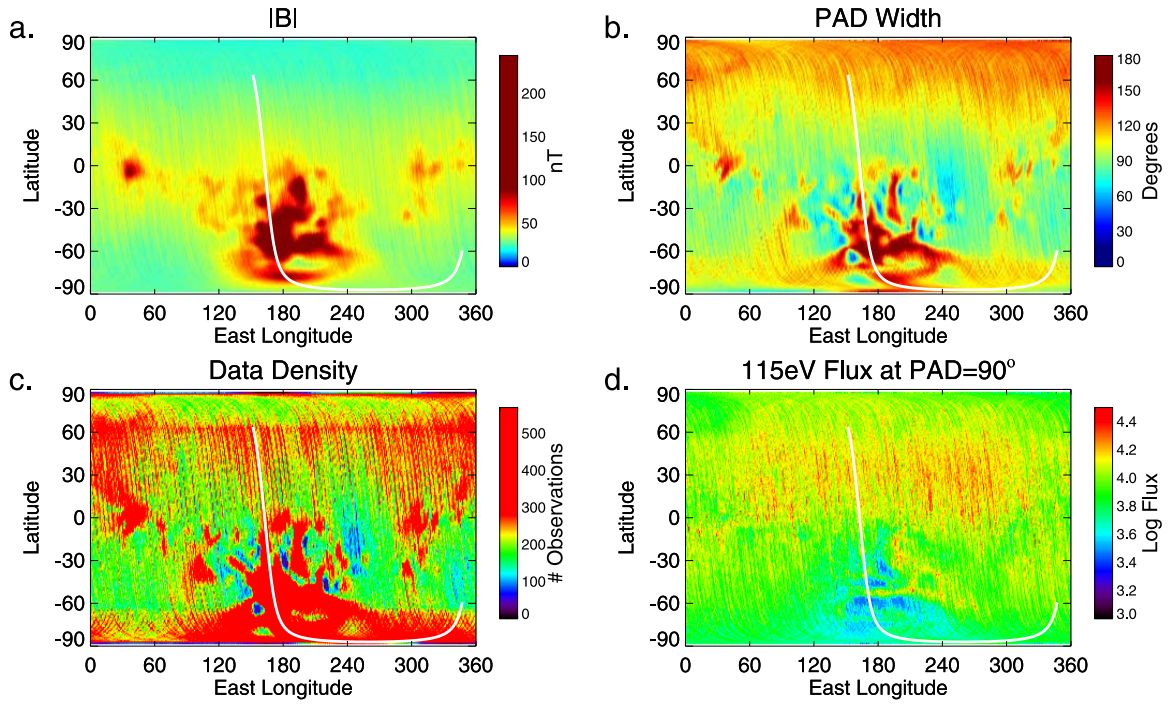

Figure 10. Dayside environment for MGS electron measurements as a function of geographic location averaged in 1° × 1° bins. (a) Average magnetic field magnitude. (b) Average pitch angle distribution width. (c) Usable data coverage. (d) Differential electron flux (number of electrons/(cm^2 s sr eV) at 90° pitch angle. The spacecraft trajectory for the pass in Figure 9 is overplotted in each panel.

directed electron flux with pitch angle within ∼45°, indicating that the flux tubes sampled by MGS intersect the collisional atmosphere. The loss cone is on opposite sides of the PAD during the two periods because the radial field component has opposite sign. We identify nearly all of these distributions as one-sided loss cones, with either isotropic or field-aligned incident flux. Photoelectron features are evident (but not prominent) in the energy spectra during these times, suggesting that a mixture of ionospheric and solar wind electrons populate these field lines.

[41] From 1621–1648 MGS passes through strong crustal fields. The width of the PAD is more variable at this time as the relative orientation of the ambient crustal fields and the ER varies. Electron fluxes decrease, though not as dramatically as for the nightside pass shown in Figure 3. Instead, very prominent photoelectron signatures (first reported by *Mitchell et al.* [2000]) are evident in the individual energy spectra at 500 eV and at ∼40 eV. The PADs are also generally more isotropic than on the nightside, as seen for much of the time period labeled "3." Several regions show evidence for loss cones in the upward directed flux at the most field-aligned pitch angles (labeled "2"), and correspond to locations where the radial component of the field is large. The loss cones are sometimes associated with changes in the energy spectrum, and the photoelectron signatures disappear or become less pronounced. We infer that MGS is often on closed magnetic field lines in strong crustal field regions isolated from the solar wind, punctuated by periods when MGS passes through cusps of vertically oriented open crustal magnetic field lines that connect to the solar wind. The isotropy of the distributions might result from a constant source of photoelectrons in the vicinity of the spacecraft, or by pitch angle scattering of mirroring electrons. Several small-scale perturbations are evident in the magnetic field components and amplitude, predominantly near cusp regions. These perturbations likely result from current systems near cusps or from enhanced wave activity in cusps.

4.2. Statistical Results

[42] We performed a statistical analysis of dayside PADs recorded by MGS, using the same time period as for the nightside analyses presented in section 3. The environment in which these observations were made is shown in Figure 10. Field strengths far from crustal sources are larger than on the nightside, and decrease at high latitudes where the compression of draped external fields is smallest (Figure 10a). Individual moderate crustal sources are more difficult to make out in observations because draped external fields are stronger on the dayside; this is also evident in the map of average PAD width (Figure 10b). Most of the pitch angle distributions measured at high latitudes and over certain crustal sources have width greater than 90°, while the sampled PADs can be much narrower near the equator. Figure 10c shows that, in general, many more observations are usable on the dayside than in eclipse. The global discontinuities at ±65° result from the 25° obliquity of Mars. Latitudes higher than ±65° spend different amounts of time with solar zenith angle more than 90° compared to midlatitudes, depending upon season. Finally, average electron fluxes at 90° pitch angle span more than an order of magnitude and are generally lower above strong crustal sources than in the weakly magnetized regions, presumably because 115 eV electrons in the solar wind have limited

Table 2. Percentage of Usable Distributions Associated With Each PAD Type When MGS Had Solar Zenith Angle <90°[a]

Return Distribution	Incident Distribution				
	Isotropic	Loss Cone	Field-Aligned Beam	Conic	Inverse Conic
Isotropic	37.5	5.7	6.2	0.7	0.3
Loss cone	18.0	5.9	7.9	0.7	0.6
Field-aligned beam	5.9	2.8	2.8	0.7	0.2
Conic	0.6	0.4	1.6	0.4	0.1
Inverse conic	0.2	0.4	0.2	0.0	0.0

[a]Incident and return PAD types are defined in text. Plasma void is 0.0% All values are given as percentages.

access to closed magnetic field lines. Note also that while fluxes are generally higher on the dayside, the highest average dayside fluxes are an order of magnitude lower than the highest average nightside fluxes.

[43] The results of classification of all usable dayside PADs is shown in Table 2. Unusable data were most often excluded because the field strength was too low to obtain a reliable pitch angle distribution (19%) or because the PAD was too narrow (31%). Voids are essentially never seen on the dayside (<7000 out of 31 million PADs), indicating electron loss processes are slower than source processes. Isotropic distributions are more common than any other type, in agreement with the case study. Isotropic distributions and field-aligned beams are more common in the incident flux than the return flux. Loss cones are more common in the return flux than the incident flux, as expected since the incident flux should only contain absorption features if a field line connects at both ends to the atmosphere.

[44] The dayside distribution of different PAD types is shown in Figure 11. Figure 11a shows the locations of two-sided loss cones and fully isotropic distributions. It is reasonable to assume that two-sided loss cones are indicative of trapped electrons on closed magnetic field lines. These make up a much smaller fraction of the PADs in Figure 11a, but are most commonly observed in the regions surrounding strong crustal magnetic field sources, as on the nightside. On the basis of examination of many orbits having similarity to Figure 9, we also assume that fully isotropic distributions indicate closed field lines. Most of these distributions are recorded at a time when the electron energy spectrum contains evidence for ionospheric photoelectrons, and the geographic distribution of the distributions resembles a map of photoelectron locations [*Mitchell et al.*, 2001b]. In some regions of strong horizontal crustal magnetic field the field topology is nearly always closed at 400 km as MGS passes through the interiors of arcades of crustal field. Several strong radial crustal field regions are only closed some of the time. This is also true above many weaker crustal fields, which may sometimes be compressed below the MGS mapping altitude on the dayside by the solar wind.

[45] Figure 11b shows the locations of one-sided loss cone distributions similar to those in the regions labeled "1" and "4" in Figure 9. One-sided loss cones populate many of the weakly magnetized regions on the dayside. The incident distribution is more often isotropic than field-aligned in Figure 11b, and is nearly always isotropic in the strong crustal field regions. We assume that the strong field regions contain open field lines that connect to the crust, and that the weakly magnetized regions contain draped field lines that intersect the atmosphere. In both cases solar wind plasma has direct access to the Martian atmosphere.

[46] Figure 12 shows a map of the dominant PAD types on the dayside, in the same style as Figure 8. Most of the dayside is dominated by two PAD types: fully isotropic distributions and isotropic incident electrons with a loss cone in the return flux. Fully isotropic distributions are concentrated near crustal magnetic fields, and likely indicate closed field lines. One-sided loss cones indicative of an open topology are dominant in the weakly magnetized northern hemisphere where draped field lines may intersect

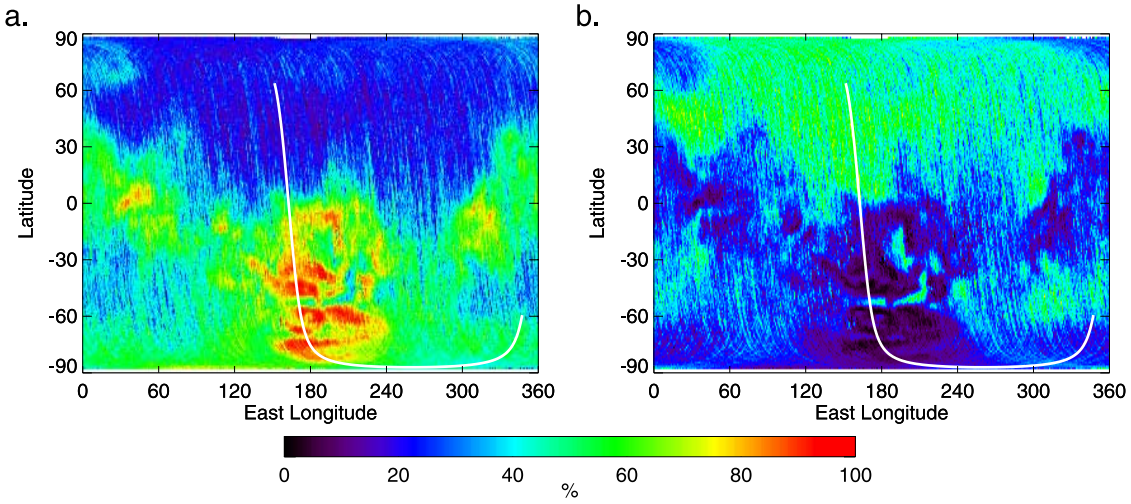

Figure 11. Frequency of occurrence of different pitch angle distribution types on the Martian dayside as a function of geographic location: (a) fully isotropic distributions and two-sided loss cones and (b) one-sided loss cones. The spacecraft trajectory for the pass in Figure 9 is overplotted in each panel.

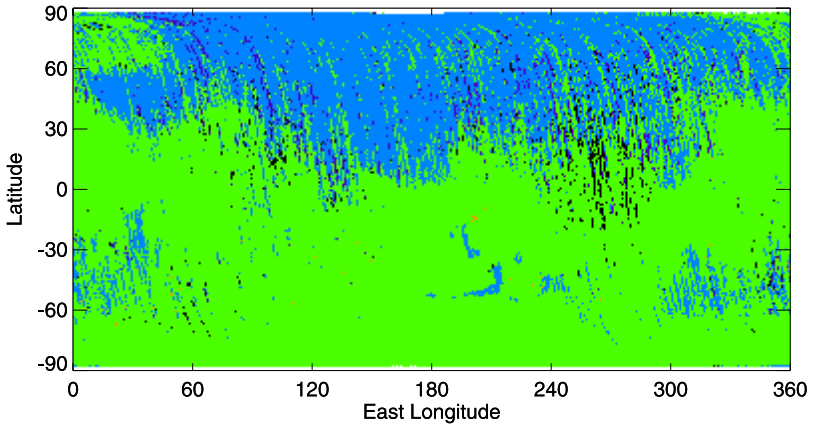

Figure 12. Geographic map of dominant PAD type recorded by MGS ER at 400 km on the dayside. Color coding is the same as for Figure 8.

the collisional atmosphere, and in cusps of strong crustal fields. A few regions in the northern hemisphere are dominated by electron populations that are field-aligned in the incident direction and have a loss cone in the return flux, indicating a streaming incident solar wind population that may intersect the atmosphere and be absorbed.

5. Summary

[47] Pitch angle distributions of 115 eV electrons recorded by MGS at 400 km altitudes over a period of 7 years have been classified according to their shape. Using more than 60 million distributions, we constructed geographic maps of the locations of closed field lines and open or unconnected field lines.

[48] Some regions on the nightside are always closed and lack any measurable electron flux. Surrounding these plasma void regions are locations where trapped (mirroring) distributions are often observed. These observations suggest that electrons populating closed field lines in sunlight are removed in darkness through a combination of outward diffusion, scattering, and interactions with the atmosphere, and that a source of electrons (reconnection or cross-field diffusion) repopulates the outer layers of closed field regions with superthermal electrons. Open field lines are more difficult to unambiguously distinguish (from unconnected field lines), but the observations strongly suggest that open magnetic field regions analogous to Earth's polar cusps are often present near strong and moderate crustal fields on the Martian nightside. In weakly and unmagnetized regions the distributions often contain evidence for atmospheric absorption features in the form of loss cones, suggesting that the draped solar wind magnetic field very often has access to the Martian nightside atmosphere.

[49] The production of ionospheric photoelectrons on the dayside complicates determination of field topology using pitch angle distributions. However, trapped distributions indicative of closed field lines are measured on the dayside near regions of strong crustal field. Also, fully isotropic distributions are also often recorded near strong crustal field regions, and might result if photoelectrons sources are isotropic at 400 km altitudes and dominate the measured electron population. Support for the association of these two distribution shapes with closed field regions comes from the geographic locations where these distributions are observed (near strong crustal fields), the orientation of the ambient field in these locations (horizontal), and the association of these regions with electron energy spectra dominated by ionospheric photoelectrons. Loss cone distributions correlate with regions of strong radial crustal field, indicating likely cusps of open magnetic field. As for the nightside, atmospheric absorption features are often evident over the weakly magnetized northern plains.

[50] Of special interest to us are regions where the pitch angle distributions indicate that the local field topology is sometimes closed and sometimes open. Further analysis of the topology in these regions, including the factors that control the topology, may reveal where and under what conditions the solar wind has access to the Martian upper atmosphere. This, in turn, has implications for the energetics of the upper atmosphere and possible atmospheric escape-related processes.

[51] In addition to examination of the factors controlling variability in the topology, the analyses here could be expanded upon in several areas in a future work. First, a more sophisticated method for identifying PAD shape and topology might be employed, allowing open and draped field lines to be distinguished from each other. Second, PADs at energies other than 115 eV should be examined to determine whether the PAD shape is similar at all energies. Third, variability in PAD type as a function of solar zenith angle for different geographic regions could be studied, including PADs recorded when MGS was in sunlight but had solar zenith angle >90° (which were not used in this analysis). Fourth, several distribution types were not explored in detail in this work and should be explained. Finally, PADs from the MGS premapping orbits could be studied to help constrain electron angular distributions and topology at Mars at altitudes and local times other than 400 km and 2 A.M./P.M.

[52] **Acknowledgments.** D.A. Brain thanks L. Peticolas, J. Luhmann, D. Crider, Tai Phan, M. Øieroset, and J. Eastwood for useful discussions. This research was supported by NASA grant NNG05GJ24G-05/07.

[53] Wolfgang Baumjohann thanks John Connerney and another reviewer for their assistance in evaluating this paper.

References

Acuña, M. H., et al. (1992), The Mars Observer Magnetic Fields Investigation, *J. Geophys. Res.*, *97*, 7799–7814.

Acuña, M. H., et al. (1998), Magnetic field and plasma observations at Mars: Initial results of the Mars Global Surveyor mission, *Science*, *279*, 1676–1680.

Acuña, M. H., et al. (1999), Global distribution of crustal magnetization discovered by the Mars Global Surveyor MAG/ER experiment, *Science*, *284*, 790–793.

Acuña, M. H., et al. (2001), The magnetic field of Mars: Summary of results from the aerobraking and mapping orbits, *J. Geophys. Res.*, *106*(E10), 23,403–23,418.

Brain, D. A. (2002), The influence of crustal magnetic sources on the topology of the Martian magnetic environment, Ph.D. thesis, Univ. of Colorado, Boulder.

Brain, D. A., F. Bagenal, M. H. Acuña, and J. E. P. Connerney (2003), Martian magnetic morphology: Contributions from the solar wind and crust, *J. Geophys. Res.*, *108*(A12), 1424, doi:10.1029/2002JA009482.

Brain, D. A., J. S. Halekas, R. J. Lillis, D. L. Mitchell, R. P. Lin, and D. H. Crider (2005), Variability of the altitude of the Martian sheath, *Geophys. Res. Lett.*, *32*(18), L18203, doi:10.1029/2005GL023126.

Brain, D. A., J. S. Halekas, L. M. Peticolas, R. P. Lin, J. G. Luhmann, D. L. Mitchell, G. T. Delory, M. H. Acuña, and H. Rème (2006), On the origin of aurorae at Mars, *Geophys. Res. Lett.*, *33*(1), L01201, doi:10.1029/2005GL024782.

Cain, J. C., B. B. Ferguson, and D. Mozzoni (2003), An $n = 90$ internal potential function of the Martian crustal magnetic field, *J. Geophys. Res.*, *108*(E2), 5008, doi:10.1029/2000JE001487.

Cloutier, P. A., et al. (1999), Venus-like interaction of the solar wind with Mars, *Geophys. Res. Lett.*, *26*(17), 2685–2688.

Connerney, J. E. P., M. H. Acuña, P. J. Wasilewski, G. Kletetschka, N. F. Ness, H. Rème, R. P. Lin, and D. L. Mitchell (2001), The global magnetic field of Mars and implications for crustal evolution, *Geophys. Res. Lett.*, *28*(21), 4015–4018.

Connerney, J. E. P., M. H. Acuña, N. F. Ness, G. Kletetschka, D. L. Mitchell, R. P. Lin, and H. Rème (2005), Tectonic implications of Mars crustal magnetism, *Proc. Natl. Acad. Sci. U. S. A.*, *102*(42), 14,970–14,975, doi:10.1073/pnas.0507469102.

Crider, D., et al. (2000), Evidence of electron impact ionization in the magnetic pileup boundary of Mars, *Geophys. Res. Lett.*, *27*(1), 45–48.

Eliasson, L., M. Andre, R. Lundin, R. Pottelette, G. Marklund, and G. Holmgren (1996), Observations of electron conics by the Viking satellite, *J. Geophys. Res.*, *101*(A6), 13,225–13,238.

Espley, J., P. A. Cloutier, D. A. Brain, D. H. Crider, and M. H. Acuña (2004), Observations of low-frequency magnetic oscillations in the Martian magnetosheath, magnetic pileup region, and tail, *J. Geophys. Res.*, *109*, A07213, doi:10.1029/2003JA010193.

Espley, J., P. A. Cloutier, D. H. Crider, D. A. Brain, and M. H. Acuña (2005), Low-frequency plasma oscillations at Mars during the October 2003 solar storm, *J. Geophys. Res.*, *110*, A09S33, doi:10.1029/2004JA010935.

Frahm, R. A., et al. (2006), Carbon dioxide photoelectron energy peaks at Mars, *Icarus*, *182*(2), 371–382, doi:10.1016/j.icarus.2006.01.014.

Gurnett, D. A., et al. (2005), Radar soundings of the ionosphere of Mars, *Science*, *310*(5756), 1929–1933, doi:10.1126/science.1121868.

Halekas, J. S., D. L. Mitchell, R. P. Lin, S. Frey, L. L. Hood, M. H. Acuña, and A. B. Binder (2001), Mapping of crustal magnetic anomalies on the lunar near side by the lunar prospector electron reflectometer, *J. Geophys. Res.*, *106*(E11), 27,841–27,852.

Halekas, J. S., D. A. Brain, R. J. Lillis, M. O. Fillingim, D. L. Mitchell, and R. P. Lin (2006), Current sheets at low altitudes in the Martian magnetotail, *Geophys. Res. Lett.*, *33*, L13101, doi:10.1029/2006GL026229.

Harnett, E. M., and R. M. Winglee (2005), Three-dimensional fluid simulations of plasma asymmetries in the Martian magnetotail caused by the magnetic anomalies, *J. Geophys. Res.*, *110*, A07226, doi:10.1029/2003JA010315.

Kahler, S. W., N. U. Crooker, and J. T. Gosling (1996), The topology of intrasector reversals of the interplanetary magnetic field, *J. Geophys. Res.*, *101*(A11), 24,373–24,382.

Krymskii, A. M., T. K. Breus, N. F. Ness, M. H. Acuña, J. E. P. Connerney, D. H. Crider, D. L. Mitchell, and S. J. Bauer (2002), Structure of the magnetic field fluxes connected with crustal magnetization and topside ionosphere at Mars, *J. Geophys. Res.*, *107*(A9), 1245, doi:10.1029/2001JA000239.

Liemohn, M. W., et al. (2006), Numerical interpretation of high-altitude photoelectron observations, *Icarus*, *182*(2), doi:10.1016/j.icarus.2005.10.036.

Lillis, R. J., D. L. Mitchell, R. P. Lin, J. E. P. Connerney, and M. H. Acuña (2004), Mapping crustal magnetic fields at Mars using electron reflectometry, *Geophys. Res. Lett.*, *31*(15), L15702, doi:10.1029/2004GL020189.

Lillis, R. J., J. H. Engel, D. L. Mitchell, D. A. Brain, R. P. Lin, S. W. Bougher, and M. H. Acuña (2005), Probing upper thermospheric neutral densities at Mars using electron reflectometry, *Geophys. Res. Lett.*, *32*(23), L23204, doi:10.1029/2005GL024337.

Luhmann, J. G., M. H. Acuña, M. Purucker, C. T. Russell, and J. G. Lyon (2002), The Martian magnetosheath: How Venus-like?, *Planet Space Sci.*, *50*, 489–502.

Ma, Y., A. F. Nagy, K. C. Hansen, D. L. DeZeeuw, and T. I. Gombosi (2002), Three-dimensional multispecies MHD studies of the solar wind interaction with Mars in the presence of crustal fields, *J. Geophys. Res.*, *107*(A10), 1282, doi:10.1029/2002JA009293.

Ma, Y., A. F. Nagy, I. V. Sokolov, and K. C. Hansen (2004), Three-dimensional, multispecies, high spatial resolution MHD studies of the solar wind interaction with Mars, *J. Geophys. Res.*, *109*, A07211, doi:10.1029/2003JA010367.

Menietti, J. D., and J. L. Burch (1985), "Electron conic" signatures observed on the nightside auroral zone and over the polar cap, *J. Geophys. Res.*, *90*(A6), 5345–5353.

Mitchell, D. G., F. Kutchko, D. J. Williams, T. E. Eastman, L. A. Frank, and C. T. Russell (1987), An extended study of the low-latitude boundary layer on the dawn and dusk flanks of the magnetosphere, *J. Geophys. Res.*, *92*(A7), 7394–7404.

Mitchell, D. L., R. P. Lin, H. Rème, D. H. Crider, P. A. Cloutier, J. E. P. Connerney, M. H. Acuña, and N. F. Ness (2000), Oxygen Auger electrons observed in Mars' ionosphere, *Geophys. Res. Lett.*, *27*(13), 1871–1874.

Mitchell, D. L., R. P. Lin, C. Mazelle, H. Rème, P. A. Cloutier, J. E. P. Connerney, M. H. Acuña, and N. F. Ness (2001a), Probing Mars' crustal magnetic field and ionosphere with the MGS Electron Reflectometer, *J. Geophys. Res.*, *106*(E10), 23,419–23,427.

Mitchell, D. L., R. P. Lin, H. Rème, P. A. Cloutier, J. E. P. Connerney, M. H. Acuña, and N. F. Ness (2001b), Probing Mars' crustal magnetic field with the MGS Electron Reflectometer, *Eos Trans. AGU*, *82*(20), Spring Meet. Suppl., Abstract GP22A–07.

Mitchell, D. L., R. J. Lillis, R. P. Lin, J. E. P. Connerney, and M. H. Acuña (2007), A global map of Mars crustal magnetic field based on electron reflectometry, *J. Geophys. Res.*, *112*, E01002, doi:10.1029/2005JE002564.

Nielsen, E., X.-D. Wang, D. A. Gurnett, D. L. Kirchner, R. Huff, R. Orosei, A. Safaeinili, J. J. Plaut, and G. Picardi (2007), Vertical sheets of dense plasma in the topside Martian ionosphere, *J. Geophys. Res.*, *112*, E02003, doi:10.1029/2006JE002723.

Priest, E., and T. Forbes (2000), *Magnetic Reconnection: MHD Theory and Applications*, Cambridge Univ. Press, New York.

Purucker, M., D. Ravat, H. Frey, C. Voorhies, T. Sabaka, and M. H. Acuña (2000), An altitude-normalized magnetic map of Mars and its interpretation, *Geophys. Res. Lett.*, *27*, 2249–2452.

Soobiah, Y., et al. (2006), Observations of magnetic anomaly signatures in Mars Express ASPERA-3 ELS data, *Icarus*, *182*(2), doi:10.1016/j.icarus.2005.10.034.

Stern, D. P., and I. I. Alexeev (1988), Where do field lines go in the quiet magnetosphere?, *Rev. Geophys.*, *26*(4), 782–791.

Vasyliunas, V. M. (1975), Theoretical models of magnetic field line merging, *Rev. Geophys.*, *13*(1), 303–336.

Willis, D. M., J. R. Singh, and J. Comer (1997), Uncertainties in field-line tracing in the magnetosphere. part I: The axisymmetric part of the internal geomagnetic field, *Ann. Geophysicae*, *15*, 165–180.

D. A. Brain, J. S. Halekas, R. J. Lillis, R. P. Lin, and D. L. Mitchell, Space Sciences Laboratory, University of California, Berkeley, 7 Gauss Way, Berkeley, CA 94720, USA. (brain@ssl.berkeley.edu)